Efficient electrical detection of ambipolar acoustic transport in GaAs

P. D. Batista,[a] R. Hey, and P. V. Santos[b]
Paul-Drude-Institut für Festkörperelektronik, Hausvogteiplatz 5-7, D-10117 Berlin, Germany

(Received 8 June 2008; accepted 16 June 2008; published online 3 July 2008)

We demonstrate a photon detector combining the ambipolar transport of electrons and holes by surface acoustic waves with electrical charge detection using a lateral *p-i-n* junction. By optimizing photon absorption and the acoustic transport, overall quantum efficiencies of 70% have been achieved for ambipolar transport lengths exceeding 100 μm. © *2008 American Institute of Physics*. [DOI: 10.1063/1.2955522]

The piezoelectric potential (Φ_{SAW}) of a surface acoustic wave (SAW) propagating on a piezoelectric semiconductor creates a dynamic type-II modulation of the energy band edges, which can be used for acoustically induced carrier transport (ACT).[1] The piezoelectric modulation is strong enough to ionize photoexcited excitons and trap the resulting electrons and holes in spatially separated regions close to the minima and maxima of the electronic energy $-e\Phi_{SAW}$, respectively, as indicated in the inset of Fig. 1(a). The spatial separation prevents recombination, so that both types of carriers can be transported over large distances (hundreds of micrometers) at the well-defined acoustic velocity.[2] The unipolar ACT of electrons as well as the ambipolar ACT of photoexcited electrons and holes have been used in fundamental investigations of the dynamics of carriers,[2–4] spins,[5–7] and excitons[8] in low-dimensional semiconductors. ACT applications include discriminating single photon detectors[9,10] as well as acoustically driven switches.[11,12]

While unipolar ACT can be easily detected by electrical means, most of the studies of ambipolar ACT have been carried out by collecting the photoluminescence (PL) emitted when the transported electrons and holes recombine. In this letter, we demonstrate an efficient process for the electrical detection of ambipolar transport based on carrier collection by a lateral *p-i-n* junction. This process is illustrated in Fig. 1. The carriers are photogenerated by a laser beam impinging at spot G on the path of a SAW generated by an acoustic interdigital transducer (IDT). The photogenerated electrons and holes are captured by Φ_{SAW} and transported toward *n*- and *p*-type doped regions, where they are collected and detected using an electrometer. The combination of ambipolar ACT with electrical detection leads to an efficient photon detector, where the processes of photon absorption, charge transport, and detection can be independently optimized. The present design is based on an (Al,Ga)As layered structure and is optimized for an operation wavelength $\lambda = 805$ nm. In order to enhance the photon-to-carrier conversion efficiency, absorption takes place within a 452-nm-thick GaAs channel layer with 48-nm-thick $Al_{0.3}Ga_{0.7}As$ barriers placed in between dielectric (Al,Ga)As Bragg mirror (BM) stacks [see Fig. 1(b)]. The lower Bragg mirror consists of 15 periods of $\lambda/4$ AlAs and $Al_{0.1}Ga_{0.9}As$ layers with thicknesses of 69 and 58 nm, respectively, producing a reflectivity stop band centered around λ. The upper mirror contains a single AlAs/$Al_{0.1}Ga_{0.9}As$ stack and is capped with a 1 nm GaAs layer. All layers are undoped and are grown on GaAs (100) using molecular beam epitaxy. The contacts to the GaAs channel were fabricated by etching the upper layers, depositing a Au–Be (Au–Ge) alloy for the *p* (*n*) contacts and alloying at 450 °C for 10 min. In order to increase the SAW generation efficiency as well as the piezoelectric field for ACT, the sample was coated with a 400-nm-thick piezoelectric ZnO layer. Finally, the IDT and the metal guides were deposited using a lift-off lithographic process. The metal guides screen the piezoelectric field underneath them, thus forcing the carriers to stay at the lower energy positions in between them during transport. Voltages applied to the gates can further help the separation of electrons and holes by attracting them to opposite sides of the transport channel.[9] In the present studies, however, this was not necessary and the gates were grounded.

Figure 2(a) displays the reflectivity *R* measured at 15 K along with a simulation using a transfer matrix approach. The measured reflectivity was normalized to that of an Al film. The sample structure forms an asymmetric optical microcavity with a 10-nm-wide reflectivity dip centered at $\lambda = 805$ nm. The calculations also yield the absorption (*A*) in the GaAs active zone (dash-dotted line), which could not be directly measured since the GaAs substrate is opaque below 820 nm. The absorption curve shows that approximately 85% of the incident photons at the maximum of the absorp-

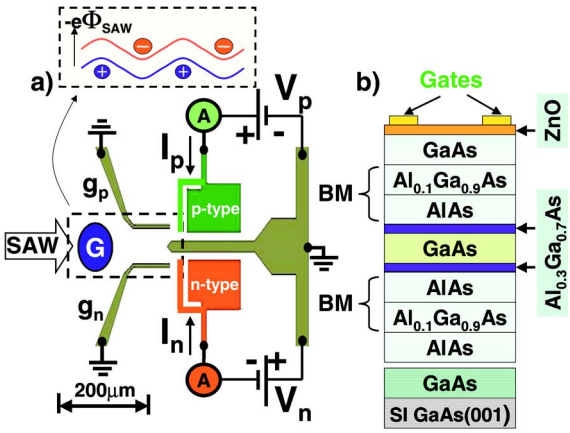

FIG. 1. (Color online) (a) Schematic view and (b) layer structure of the detector grown on a semi-insulating GaAs (100) substrate. Electrons and holes photoexcited at G are transported by the SAW [see the inset of (a)] in the channel in between the metal guides (g_n and g_p) toward the charge detection areas formed by the *p*- and *n*-type contacts.

[a]Present address: Univ. de São Paulo, Dep. de Física e Matemática, Av. Bandeirantes 3900, 14040-901 Ribeirão Preto, SP, Brazil.
[b]Electronic mail: santos@pdi-berlin.de.

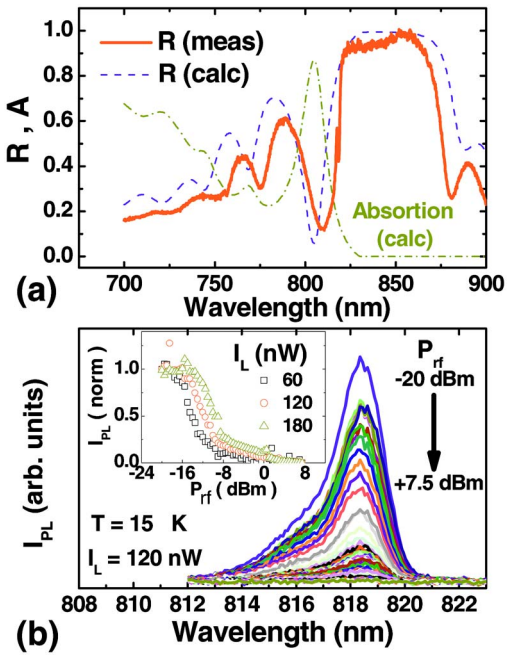

FIG. 2. (Color online) (a) Measured (red solid line) and calculated (blue dashed line) optical reflectivity R as well as the calculated absorptivity (A, dash-dotted line) of the structure in Fig. 1(b). (b) PL spectra at the generation point G as a function of the nominal rf power applied to the IDT (P_{rf}) for a light excitation intensity I_L=120 nW. The inset shows the PL intensity (I_{PL}) at 818.2 nm as a function of I_L and P_{rf}.

tion peak are converted into electron-hole pairs in the GaAs channel.

The ACT investigations were carried out at 15 K using a setup for microscopic optical measurements. The samples are mounted in a continuous flow He cryostat with feedthroughs for electrical connections and for the radio-frequency (rf) excitation of the IDTs. The photon-to-carrier conversion was studied using spectroscopic PL excited by a 760 nm pulsed laser delivering 100 ps pulses at a repetition rate of 20 MHz. The measurements were carried out using a confocal setup with generation and detection spots with a diameter of approximately 2 μm. Figure 2(b) displays PL spectra recorded at the generation point G [see Fig. 1(a)] for different nominal acoustic powers (P_{rf}) applied to the IDT. The PL consists of a peak at the GaAs excitonic emission wavelength (818.2 nm) with a tail toward higher energy. The asymmetric line shape is attributed to the distortion introduced by the cavity resonance [see Fig. 2(a)]. The PL intensity reduces with P_{rf} and practically disappears for $P_{\mathrm{rf}}>7$ dBm, as indicated in the inset. The quenching of the PL is attributed to the ionization of the photoexcited excitons and the subsequent extraction of the resulting electrons and holes from the generation area by the SAW field.

The electrical response of the detector was accessed by generating carriers within a 2-μm-wide spot G located approximately 250 μm away from the p-i-n junction and by detecting the currents I_n and I_p at the n and p contacts, respectively [see Fig. 1]. Optical excitation was provided by a pulsed laser emitting close to the reflectivity dip in Fig. 2(b) (at 805 nm). The corresponding photon energy is below the band gap of the $Al_{0.1}Ga_{0.9}As$ layers of the Bragg mirrors, so that the carriers are selectively absorbed in the GaAs channel. In order to collect the transported electrons and holes, the p-i-n junction was biased with a voltage $V_{pn}=V_p-V_n$ with $V_n=-V_p$, where V_n (V_p) denotes the voltage applied between the n (p) contact and ground [see Fig. 1(a)].

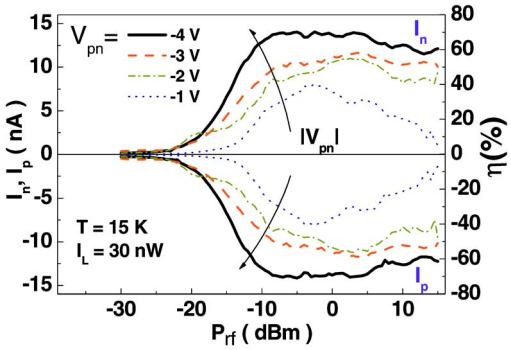

FIG. 3. (Color online) Dependence of the currents I_n and I_p on acoustic power P_{rf} for different voltages $V_{pn}=V_p-V_n$ applied to the contacts [see Fig. 1(a)]. The right vertical scale shows the collection efficiency η [see Eq. (1)]. The experiments were carried out at 15 K with the laser spot (I_L =30 nW) located 250 μm away from the contacts.

Figure 3 displays the currents I_n and I_p as a function of P_{rf} and V_{pn} for a laser excitation spot with power I_L =30 nW located 250 μm away from the contacts. For all applied voltages, the dark current of the p-i-n junction remains below 10 pA, a value much smaller than the photocurrent. Note that $I_n=-I_p$ over the whole range of rf powers, as expected for the collection of the equal numbers of electrons and holes generated by the incident beam. In order to quantify the detector performance, the right vertical scale displays the photon collection efficiency (or detector quantum efficiency) η. For a given illumination position, η is defined as the ratio between the number (per unit time) of detected electron-hole pairs ($N_{e,h}$) and the one of incident photons flux (N_{ph}) according to

$$\eta=\frac{N_{e,h}^{c}}{N_{\mathrm{ph}}}=\frac{\hbar\omega_L}{e}\frac{I_{p(n)}}{I_L}, \tag{1}$$

where $\hbar\omega_L$ is the photon energy. Note that η represents a lower limit for the internal quantum efficiency since it does not take into account losses due to reflection or incomplete photon absorption in the active layer.

For low rf powers ($P_{\mathrm{rf}}<-20$ dBm), η is very small since the SAW fields are not strong enough to trap and transport the carriers. The efficiency increases for $-20<P_{\mathrm{rf}}<-10$ dBm and reaches a maximum value for $V_{pn}=-4$ V and $-10<P_{\mathrm{rf}}<5$ dBm.[13] Within this power range, the overall quantum efficiency approaches 70%. Due to the screening of the piezoelectric potential by the photoexcited carriers, the rf-power dependence shifts to high power levels with the illumination intensity. It is interesting to note that for low values of V_{pn} the efficiency reduces for high rf powers. PL images recorded under these conditions indicate an enhanced recombination close to the metal guides (not shown here). Further investigations are required to understand this behavior.

Assuming a photon-to-carrier conversion efficiency of 85% [see Fig. 2(a)] and an overall efficiency η=70%, we estimate that at least η_t=82% of the carriers generated at G reaches the p-i-n junction, which is located 250 μm away from G [see Fig. 1(a)]. More reliable values for transport efficiency η_t can be obtained by measuring the contact current I_n while scanning the laser spot over the detector area.

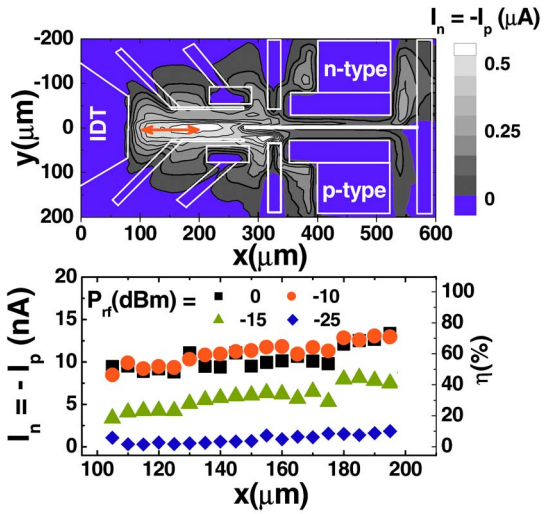

FIG. 4. (Color online) (a) Two-dimensional plot of I_n ($=-I_p$) recorded at $T=15$ K while scanning a 2-μm-wide laser spot ($I_L=600$ nW) over the detector [see Fig. 1(a)]. The outlined regions indicate the metallization areas. (b) Current profile recorded along the arrow at $y=0$ in (a) with $I_L=30$ nW, $V_{pn}=-4$ V, and $P_{rf}=0$ dBm. The right scale indicates the collection efficiency.

Figure 4(a) displays a two-dimensional profile of I_n obtained by scanning a laser spot with intensity $I_L=600$ nW over the detector area [see Fig. 1(a)]. The collected current is small away from the SAW beam as well as underneath the metallized regions, which are indicated by the outlines. As expected, the areas with high collection efficiency are found in between the guides. Figure 4(b) displays an I_n profile recorded with $I_L=30$ nW along the SAW path in the region in between the guides [indicated by the arrow in Fig. 1(a)]. For rf powers between −10 and 0 dBm, the collection efficiency lies between 50% and 65% for positions between 100 and 200 μm. From the slope of the curves obtained under these conditions, we estimate that at most 12% of the carriers are lost during transport over a distance of 100 μm, thus leading to transport efficiencies close to 90%. The transport losses are attributed to the trap of carriers of one polarity and their recombination with carriers of the opposite polarity at a subsequent SAW half-cycle [see the inset of Fig. 1(a)].

In conclusion, we have demonstrated a photon detector based on the electrical detection of the ambipolar ACT using a lateral *p-i-n* junction. The measured quantum efficiencies of approximately 70% open the way for the use of ACT in efficient optoelectronic devices.

We thank U. Jahn and E. Cerda for comments and for a critical reading of the manuscript as well as M. Höricke, B. Drescher, and W. Seidel for the sample fabrication. We also acknowledge support from the DAAD-CAPES Germany/Brazil and from the "ACDET II" European project.

[1] N. J. Moll, O. W. Otto, and C. F. Quate, J. Phys. Colloq. **33**, 231 (1972).
[2] C. Rocke, S. Zimmermann, A. Wixforth, J. P. Kotthaus, G. Böhm, and G. Weimann, Phys. Rev. Lett. **78**, 4099 (1997).
[3] J. M. Shilton, V. I. Talyanskii, M. Pepper, D. A. Ritchie, J. E. F. Frost, C. J. B. Ford, C. G. Smith, and G. A. C. Jones, J. Phys.: Condens. Matter **8**, L531 (1996).
[4] J. A. H. Stotz, F. Alsina, R. Hey, and P. V. Santos, Physica E (Amsterdam) **26**, 57 (2005).
[5] J. A. H. Stotz, R. Hey, P. V. Santos, and K. H. Ploog, Nat. Mater. **4**, 585 (2005).
[6] O. D. D. Couto, Jr., F. Iikawa, J. R. R. Hey, and P. V. Santos, Phys. Rev. Lett. **98**, 036603 (2007).
[7] S. V. T. Hosey, V. Talyanskii, G. A. C. Jones, M. B. Ward, D. C. Unitt, C. E. Norman, and A. J. Shields, Appl. Phys. Lett. **85**, 491 (2004).
[8] J. Rudolph, R. Hey, and P. V. Santos, Phys. Rev. Lett. **99**, 047602 (2007).
[9] V. I. Talyanskii, G. J. Milburn, J. A. H. Stotz, and P. V. Santos, Jr., Semicond. Sci. Technol. **22**, 209 (2007).
[10] P. D. Batista, M. Gustafsson, M. M. de Lima, Jr., M. Beck, V. I. Talyanskii, R. Hey, P. V. Santos, M. P. Delsing, and J. Rarity, Proc. SPIE **6583**, 658304 (2007).
[11] V. I. Talyanskii, M. R. Graham, and H. E. Beere, Appl. Phys. Lett. **88**, 083501 (2006).
[12] M. M. de Lima, Jr., R. Hey, J. A. H. Stotz, and P. V. Santos, Appl. Phys. Lett. **84**, 2569 (2004).
[13] The increase in the reverse current (see inset of Fig. 3) limits V_{pn} to values >-4 V.